Journal of Cardiovascular Magnetic Resonance 27 (2025) 101901

Contents lists available at ScienceDirect

Journal of Cardiovascular Magnetic Resonance

journal homepage: www.sciencedirect.com/journal/jocmr

Original Research

Free-breathing single-beat exercise cardiovascular magnetic resonance with generative artificial intelligence for evaluation of volumetric and functional cardiac indices: A reproducibility study

Fahime Ghanbari[a], Alexander Schulz[a], Manuel A. Morales[a], Jennifer Rodriguez[a], Jordan A. Street[a], Kathryn Arcand[a], Scott Johnson[a], Patrick Pierce[a], Christopher W. Hoeger[a], Connie W. Tsao[a], Warren J. Manning[a,b], Reza Nezafat[a,*]

[a] Department of Medicine (Cardiovascular Division), Beth Israel Deaconess Medical Center and Harvard Medical School, Boston, Massachusetts, USA
[b] Department of Radiology, Beth Israel Deaconess Medical Center and Harvard Medical School, Boston, Massachusetts, USA

ARTICLE INFO

Keywords:
Exercise-CMR
Free-breathing single-beat cine
Biventricular volumetric and functional indices

ABSTRACT

Background: Exercise cardiovascular magnetic resonance (Ex-CMR) can reveal pathophysiologies not evident at rest by quantifying biventricular volume and function during or immediately after exercise. However, achieving reproducible Ex-CMR measurements is challenging due to limited spatial and temporal resolution. This study aimed to develop and evaluate a free-breathing, high-spatiotemporal-resolution single-beat Ex-CMR cine enhanced by generative artificial intelligence. We assessed image analysis reproducibility, scan-rescan reproducibility, and impact of the reader's experience on the analysis.

Methods: Imaging was performed on a 3T CMR system using a free-breathing, highly accelerated, multi-slice, single-beat cine sequence (in-plane spatiotemporal resolution of 1.9 × 1.9 mm^2 and 37 ms, respectively). High acceleration was achieved by combining compressed sensing reconstruction with a resolution-enhancement generative adversarial inline neural network. Ex-CMR was performed using a supine ergometer positioned immediately outside the magnet bore. Single-beat cine images were acquired at rest and immediately post-exercise. In a prospective study, the protocol was evaluated in 141 subjects. A structured image analysis workflow was implemented. Four expert readers, with or without prior training in single-beat Ex-CMR, independently rated all images for diagnostic and image quality. The subjective assessment used two 3-point Likert scales. Biventricular parameters were calculated. Inter- and intra-observer reproducibility were assessed. Fifteen healthy subjects were re-imaged 1 year later for scan-rescan reproducibility. Reproducibility was assessed using intraclass correlation coefficient (ICC), with agreement evaluated via Bland-Altman analysis, linear regression, and Pearson correlation.

Results: Free-breathing, single-beat Ex-CMR cine enabled imaging of the beating heart within 30 ± 6 s, with technically successful scans in 96% (136/141) of subjects. Post-exercise single-beat cine images were assessed as diagnostic in 98% (133/136), 96% (131/136), 82% (112/136), and 65% (89/136) of cases by four readers (ordered by descending years of Ex-CMR experience). Good image quality was reported in 74% (100/136) to 80% (109/136) of subjects. Biventricular parameters were successfully measured in all subjects, demonstrating good to excellent inter-observer reproducibility. Scan/rescan reproducibility over 1 year, assessed by two independent readers, showed excellent inter-visit ICCs (0.96–1.0) and strong correlations ($R^2 \geq 0.92$, $p < 0.001$ for left ventricle; $R^2 \geq 0.95$, $p < 0.001$ for right ventricle).

Conclusion: Single-beat Ex-CMR enabled evaluation of biventricular volumetric and functional indices with excellent reproducibility.

Abbreviations: AI, artificial intelligence; CS, compressed sensing; DL, deep learning; EDV, end-diastolic volume; EF, ejection fraction; ESV, end-systolic volume; HR, heart rate; LV, left ventricle/ventricular; MPHR, maximum age-predicted heart rate; REGAIN, resolution-enhancement generative adversarial inline neural network; RV, right ventricle/ventricular; PVC, premature ventricular contractions; SV, stroke volume; WMA, wall motion abnormality; Ex, exercise; CMR, cardiovascular magnetic resonance; ICC, intra-class correlation coefficient; ECG, electrocardiogram; HF, heart failure; CAD, coronary artery disease; FIRE, framework for image reconstruction; CI, confidence interval; WMA, wall motion abnormalities

* Corresponding author.
E-mail address: rnezafat@bidmc.harvard.edu (R. Nezafat).

https://doi.org/10.1016/j.jocmr.2025.101901
Received 7 February 2025; Received in revised form 16 April 2025; Accepted 24 April 2025
1097-6647/© 2025 The Author(s). Published by Elsevier Inc. on behalf of Society for Cardiovascular Magnetic Resonance. This is an open access article under the CC BY-NC-ND license (http://creativecommons.org/licenses/by-nc-nd/4.0/).

1. Background

Since its introduction over two decades ago [1], exercise cardiovascular magnetic resonance (Ex-CMR) has evolved significantly, driven by technical advancements and expanding clinical applications [2,3]. Combining physiological stress with CMR, Ex-CMR can detect pathophysiological changes not apparent at rest, providing valuable insights into cardiomyopathies, therapeutic responses, and prognostic outcomes [2–11].

Rest cine imaging is the non-invasive gold standard for biventricular volumetric and functional assessment [12–14]. However, achieving accurate volumetric and functional measurements during Ex-CMR using traditional breath-holding [15,16] or electrocardiogram-gated (ECG) cine techniques [17,18] is challenging, as breath-holding during exercise is difficult, and ECG gating issues often compromise image quality. Traditional resting cine imaging relies on ECG-gated acquisition and retrospective gating, requiring regular heart rhythm, repeated breath-holding, and high patient cooperation—limitations hindering its application in Ex-CMR [19]. These limitations have so far prevented a systematic assessment of cardiac volumetric adaptation to physiological stress, which may improve the phenotyping of cardiac patients. Therefore, there is an unmet need to implement a cine sequence for Ex-CMR and assess its feasibility and reproducibility of volumetric and functional indices when the cardiovascular system is stressed.

Real-time cine imaging, with continuous image acquisition during free breathing, has been used in Ex-CMR protocols [6]. However, balancing spatial and temporal resolution with scan time remains challenging, limiting the accuracy of volumetric and functional assessments during Ex-CMR. Accelerating imaging techniques through compressed sensing (CS) has improved spatial or temporal resolution [20,21]. Still, it remains limited by reduced image sharpness, long reconstruction time, and limited signal-to-noise ratio, particularly at higher acceleration rates [22]. Multiple motion-correction CS methods have been introduced [23–26]; however, their lengthy reconstruction times have hindered widespread adoption.

Deep learning (DL) reconstruction methods, utilizing algorithms such as U-net [27–30] and unrolled networks [31,32], have shown promise in accelerating cine imaging. Additionally, super-resolution algorithms [33,34] benefit from generative artificial intelligence (AI)

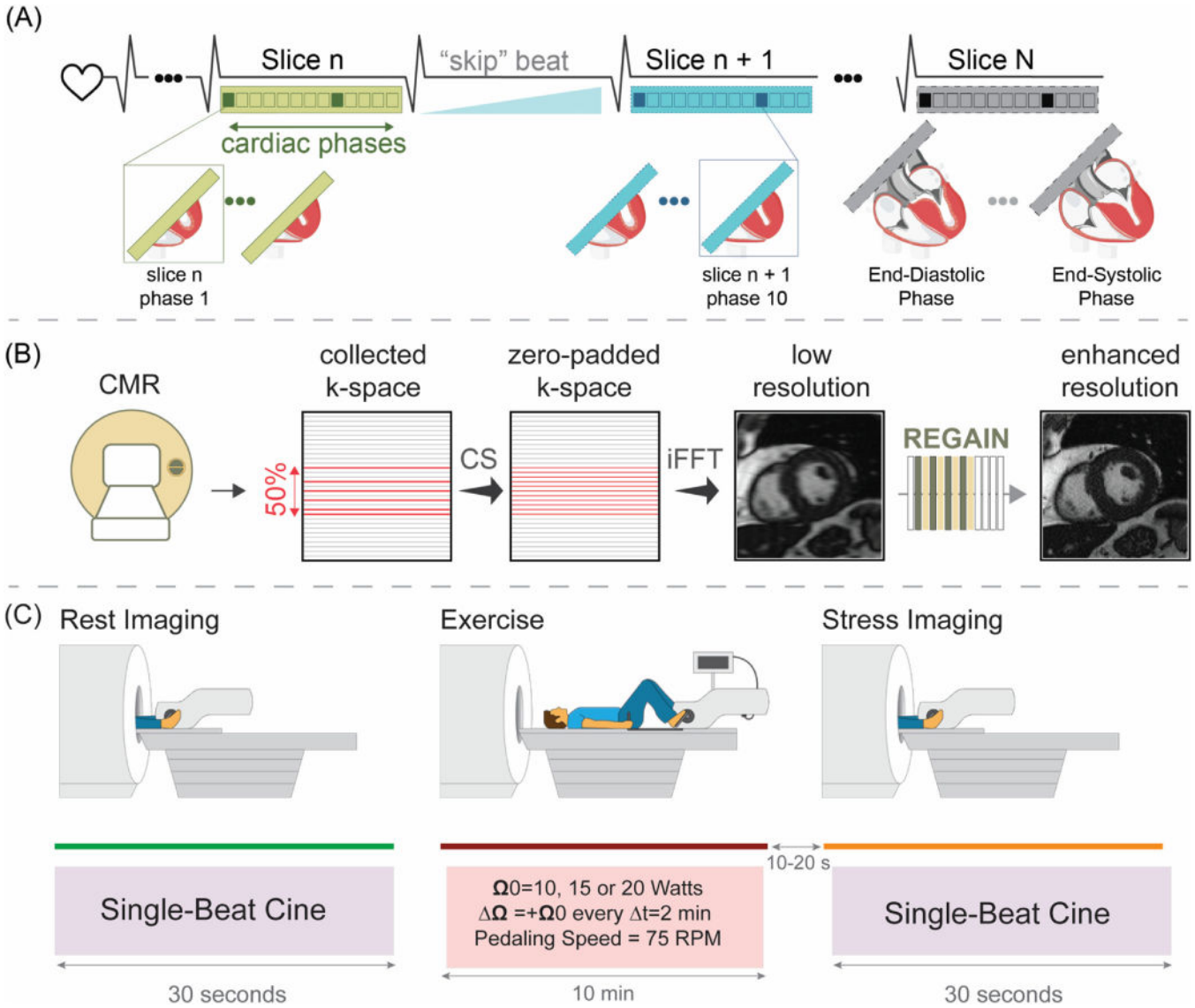

Fig. 1. (A) Free-breathing, ECG-triggered, single-beat cine acquisition collects data for each slice in one heartbeat. A dummy heartbeat is used to take the magnetization to steady-state. (B) Image reconstruction pipeline with non-uniform k-space sampling. Low-resolution images are enhanced with REGAIN. REGAIN processes each image in 32 ms, with data transfer between the external server and scanner console taking 4.6 ms per image. (C) Exercise protocol using identical cine imaging for rest and stress imaging. *ECG* electrocardiogram-gated, *REGAIN* resolution-enhancement generative adversarial inline neural network, *CMR* cardiovascular magnetic resonance, *CS* compressed sensing, *iFFT* inverse Fast Fourier Transform.

advancements that improve image quality [34,35], enabling seamless integration without requiring sequence modifications [36]. These rapid reconstruction techniques are particularly suited for real-time cine imaging, but data on their application in Ex-CMR remain limited.

Building on recent advances in generative AI, we implemented a free-breathing, high-spatiotemporal resolution, prospectively ECG-triggered, single-beat cine sequence with a dedicated analysis workflow [36,37]. This sequence was recently compared to ECG-gated cine for rest CMR, demonstrating a strong correlation in biventricular indices, along with excellent reproducibility and good image quality [37]. In this study, we assess the feasibility, reproducibility, and image quality of this approach for Ex-CMR cine, using a structured data analysis workflow. Our primary objective is to evaluate the feasibility of volumetric measurements using our physiological stress CMR protocol.

2. Methods

2.1. Participants

Our local institutional review board approved this Health Insurance Portability and Accountability Act-compliant study. The study included healthy subjects with no cardiac conditions who led active lifestyles and patients with known or suspected cardiovascular disease. Participants were recruited from July 2022 to December 2024. All participants provided written informed consent. For the patient cohorts, we included dyspneic patients with either established heart failure (HF) or those undergoing evaluation for dyspnea of unknown etiology. The inclusion criteria were dyspneic patients aged 18–80 years and able to perform a supine bike exercise. Exclusion criteria included CMR contraindications, presence of an intracardiac device, moderate or greater valvulopathy, hypertrophic cardiomyopathy, and coronary artery disease (CAD) requiring revascularization or intervention. Patients with cines acquiring incomplete capture cycles, premature ventricular contractions (PVCs), or those acquired with non-sinus rhythm at the time of scanning were excluded from final analyses.

2.2. Free-breathing single-beat cine

Fig. 1A illustrates the schematic of the free-breathing, prospectively ECG-triggered, multi-slice single-beat cine acquisition (hereafter referred to as single-beat cine). A detailed description of the development process for the single-beat cine sequence has been previously reported

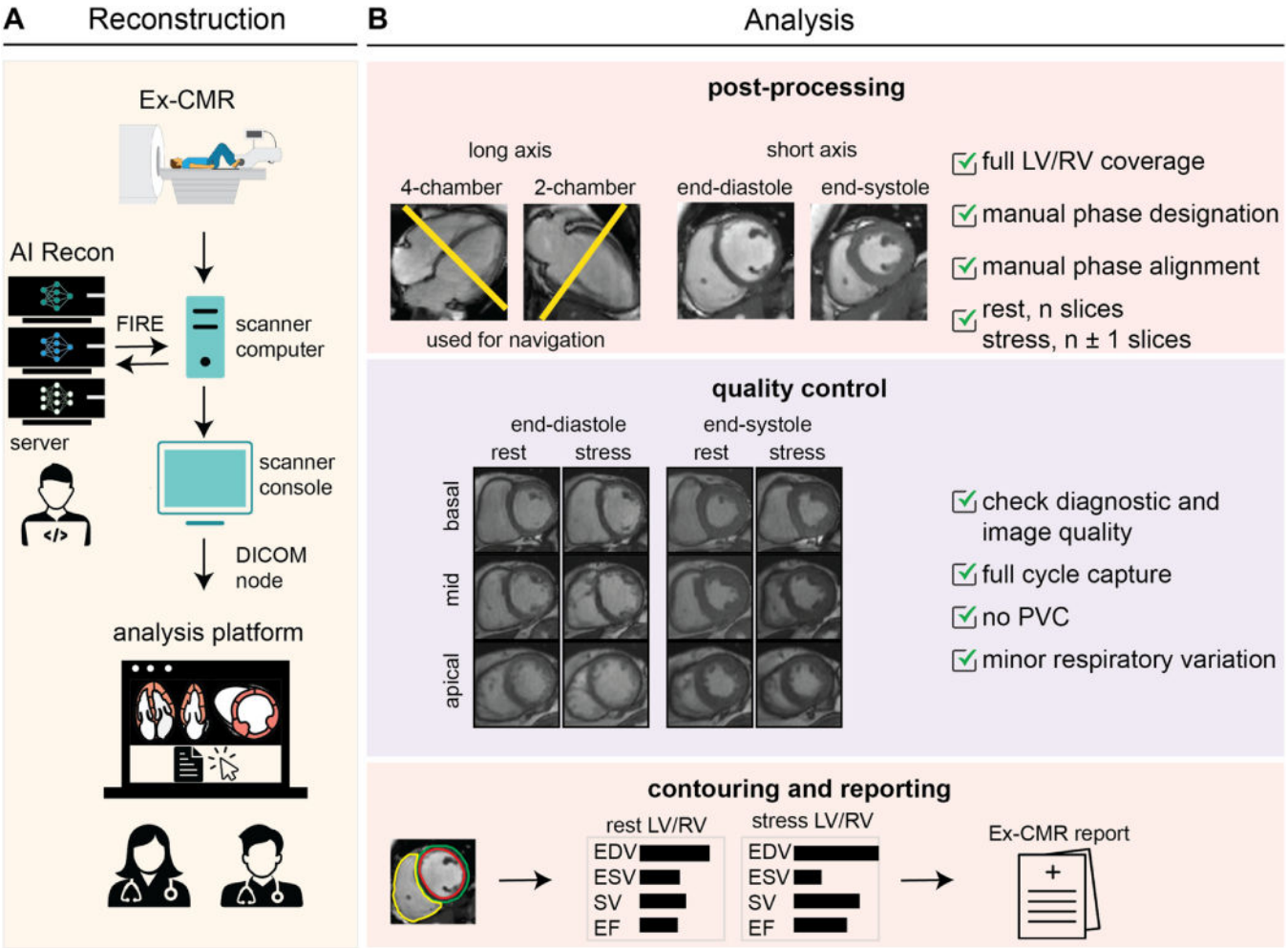

Fig. 2. (A) Reconstruction pipeline: data from Ex-CMR is sent to the Framework for Image Reconstruction (FIRE) and then to an external server for AI processing. Reconstructed images are returned to the scanner console in DICOM format for immediate display. (B) Image analysis workflow: preprocessing and quality control ensure consistency in cardiac phases and enable precise rest-stress comparisons. LV and RV basal/apical slices are identified for full biventricular coverage, particularly in stress images where post-exercise displacement may occur. End-systole and end-diastole are manually designated, and selected images are transferred to a new series for alignment and analysis, with two frames per slice. Rigorous quality control confirms the feasibility of endocardial tracing, complete cycle capture, and absence of PVCs, ensuring matched slices and minimal respiratory variation. *EDV* end-diastolic volume, *EF* ejection fraction, *ESV* end-systolic volume, *LV* left ventricle, *PVC* premature ventricular contraction, *RV* right ventricle, *SV* stroke volume, *Ex-CMR* exercise cardiovascular magnetic resonance, *DICOM* digital imaging and communications in medicine

[37]. We applied this sequence to the Ex-CMR protocol without modifying the imaging parameters (Table S1). In brief, the sequence acquires cine data for each slice following an ECG trigger in a single-shot fashion. A dummy heartbeat is used for each slice to establish a steady state. Therefore, for collecting N slices, this approach requires 2 × N heartbeats. High acceleration is achieved by using CS image reconstruction followed by applying resolution-enhancement generative adversarial inline neural network (REGAIN) (Fig. S1) [36]. This approach achieved a 14.8-fold acceleration compared to fully sampled k-space.

Figs. 1B and 2A show our image reconstruction pipeline. Single-beat cine images are prescribed at a low spatial resolution along the phase-encode direction. A vendor-provided CS reconstruction is used to reconstruct low-resolution images. The low-resolution images are then input to REGAIN to improve image sharpness. REGAIN is integrated with the scanner using the Siemens Framework for Image Reconstruction (FIRE) prototype [38]. Images were reconstructed inline (i.e., in-scanner) immediately after data collection and were transferred to a stand-alone analysis workstation for further analysis.

2.3. Image acquisition

Imaging was performed on a 3T CMR system (MAGNETOM Vida, Siemens Healthineers AG, Forchheim, Germany). Cine images were acquired using a balanced steady-state free precession readout in short-axis and long-axis orientations. Two cine imaging datasets were acquired for each subject (Fig. 1C), using the single-beat cine, covering the entire heart: one at rest and the other immediately (within 10–20 s) post-exercise, referred to as rest and stress single-beat cine imaging, respectively. The baseline cine characteristics in this study are also reported using single-beat cine. We recently conducted a systematic comparison between rest single-beat cine and ECG-gated cine in the same population, demonstrating no significant differences in biventricular ejection fraction (EF), despite a slight tendency toward overestimation of volumes during free-breathing [37].

2.4. Scan/rescan reproducibility

A subset of healthy subjects (n = 15) was invited to return 1 year later for a second Ex-CMR study, where they underwent the identical single-beat Ex-CMR protocol to assess inter-visit reproducibility. In addition, we repeated the resting scans twice during the second visit (i.e., Rest1, Rest2) before initiating the exercise protocol, observing the trends in volumetric and functional changes across the three scans (i.e., Rest1, Rest2, and Stress).

2.5. Exercise protocol

Fig. 1C shows the exercise protocol. The utilized supine bicycle ergometer protocol involved subjects exercising on the scanner table immediately outside the scanner bore using a CMR-compatible cycle ergometer (Lode, Groningen, The Netherlands) attached to the scanner table. Work rate began at Ω and increased by $\Delta\Omega = +\Omega$ every 2 min, maintaining a constant pedaling speed of 75 rpm. Subjects followed Ω = 10–20 W resistance protocols. Upon exhaustion or after a 10-minute exercise interval, subjects were immediately returned to the scanner bore for stress imaging, with a 10–20 s gap between peak exercise and the start of stress imaging. Subsequently, cine images were promptly collected. During supervised exercise, at each workload stage, participants were asked to rate their subjective perception of exercise intensity using the following scale: (1) easy, (2) easy to moderate, (3) moderate, (4) moderate to hard, (5) hard, and (6) very hard. Vital signs, including heart rate (HR), were monitored and recorded at each incremental step and during recovery. In addition, HRs were recorded during each cine acquisition.

2.6. Image analysis workflow

Fig. 2B illustrates our image analysis workflow, outlining the step-by-step process. This workflow enabled: (a) addressing potential cardiac phase inconsistencies between slices, common in real-time cine imaging, through manual designation and alignment of cardiac phases for both resting and stress imaging, (b) ensuring full biventricular coverage for measurements, particularly for stress imaging where patient displacement during exercise is possible, (c) rigorous quality control to evaluate diagnostic and image quality, as well as to confirm complete cycle capture and the absence of PVCs, especially in stress imaging, and (d) a head-to-head structural and respiratory comparison between rest and stress images, ensuring matched slices and minimal respiratory variation. To ensure consistency in quantification, readers were instructed to assign end-diastole (ED) and end-systole (ES) to the second RR interval in each slice if more than one RR interval was acquired, provided there was no presence of PVC or incomplete cycle capture. The selected ED and ES were then used for both LV and RV measurements. While this approach promotes consistency among readers and measurements, it may introduce potential over- or underestimation of volumes in a specific slice depending on the timing within the respiratory cycle and the slice profile of each acquisition. To minimize this, if readers visually observed significant respiratory variation, they were instructed to select the ED/ES of an RR interval with the least respiratory variation.

2.7. Qualitative assessments

The qualitative assessments utilized two Likert scales to evaluate diagnostic and image quality. Four independent readers rated the cine images. Readers were instructed to first perform a subjective assessment to interpret the images for diagnostic quality by playing the cine videos, visually evaluating structural aspects, and assigning a score within seconds. They then assessed only static images for quality and blurring, conducting a more detailed evaluation of endocardial and epicardial borders to identify artifacts and determine the feasibility of contouring—crucial for volumetric calculation. Quality assessment also involved manual adjustment of the window level. For artifact assessment, readers were instructed to focus on blurring and separately note any artifacts beyond that. Detailed scoring criteria are provided in Table 1. A 3-point scale was used for diagnostic quality (1 = diagnostic, 2 = non-confident, 3 = non-diagnostic), and another for image quality (1 = good, 2 = adequate, 3 = poor). The objective of the qualitative assessment was twofold: (a) to explore the clinically relevant implications of Ex-CMR single-beat imaging and evaluate its different aspects within the limits of our study design and (b) to gather subjective perspectives from readers with varying levels of single-beat Ex-CMR analysis experience. To achieve this, we developed this clinically oriented scoring system emphasizing the feasibility of accurate endocardial contouring, which is essential for reliable volumetric assessment. We selected readers with varying levels of experience in single-beat Ex-CMR cine interpretation. All readers were skilled in standard CMR analysis, but their experience with single-beat Ex-CMR varied. Reader experience is represented by two metrics: the first indicates years of experience in CMR analysis, and the second shows the number of single-beat Ex-CMR cines analyzed quantitatively. F.G. (8 years, 250 Ex-CMR cines), A.S. (8 years, 100 Ex-CMR cines), C.H. (3 years, 20 Ex-CMR cines), and C.T. (15 years, 0 Ex-CMR cines). Fig. 3 presents representative images categorized as good, adequate, and poor quality.

2.8. Quantitative assessments

The quantitative assessments of single-beat Ex-CMR cine included four parts: (1) an expert reader (F.G.), with 8 years of experience in CMR, measured all biventricular parameters (end-systolic volume [ESV], end-diastolic volume [EDV], stroke volume [SV], and EF) across

Table 1
Scoring criteria.

Diagnostic quality scoring[*] (3-point Likert scale)
Criteria
a. Tracking of wall motion abnormalities is feasible.
b. Visual estimation of ventricular ejection fraction is feasible.
c. Structural evaluation (e.g., hyper-trabeculations and wall thickness) is feasible.
The cine images are scored by the reader as
1 = Diagnostic if all the above criteria were met.
2 = non-confident for diagnostic if one or two of the criteria were missing.
3 = non-diagnostic when all criteria failed.
Image quality scoring[†] (3-point Likert scale)
1 = good; negligible to mild blurring may be present but is limited to less than half of the circumferential field of view in each image field and/or fewer than half of the slices. The border between the blood pool and myocardium is sharp, facilitating undisturbed analysis. Both the endocardial and epicardial borders can be clearly delineated.
2 = adequate; artifacts, predominantly blurring, affect over half of the field of view per image or more than half of the slices per acquisition. This disrupts epicardial contour delineation, but endocardial contour delineation remains feasible.
3 = poor; artifacts are universally present in all images, disrupting the delineation of both epicardial and endocardial contours in each instance.

[*] Readers were instructed to disregard occasional occurrences of magnetization instability affecting the initial RRs. If evident, they were tasked with assessing cine loops starting from the second RR interval in such cases

[†] Readers were instructed to evaluate image quality, specifically focusing on the degree of blurring and its impact on end-diastolic and end-systolic images, as well as the feasibility of accurate contouring

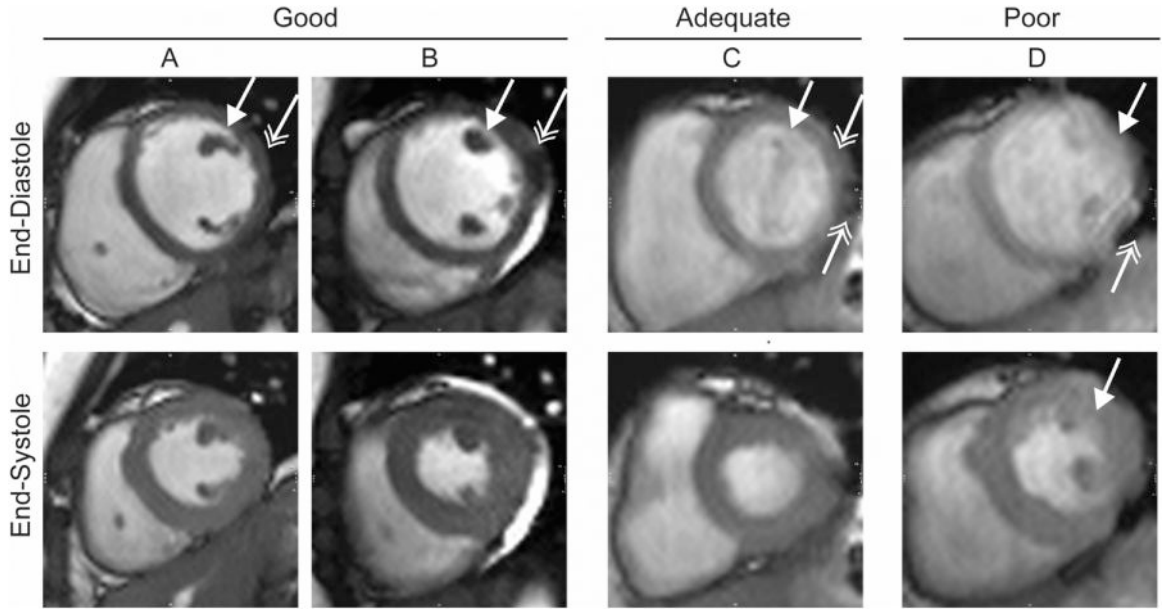

Fig. 3. Four representative examples of image quality assessment in free-breathing single-beat acquisition are presented. Endocardial borders (white filled arrows) and epicardial borders (narrow white arrows) are emphasized. In images labeled as good (panels A and B), well-defined borders are observed at both endocardial and epicardial levels. In images in panel B, despite the chemical shift artifact close to the epicardial border, delineation of the epicardial border is feasible. In images labeled as adequate (panel C), blurring intensity increases, mainly disturbing epicardial tracing. However, endocardial tracing, despite blurring, remains feasible, allowing accurate volumetric assessment. In images labeled as poor (panel D), both epicardial and endocardial tracing are impaired

all subjects, utilizing cvi42 software (version 6.0.2, Circle Cardiovascular Imaging Inc., Calgary, Alberta, Canada); (2) reader 2 (A.S.), with 8 years of experience (Society for Cardiovascular Magnetic Resonance level 3), independently measured these parameters in a random sample of 41 cases (30%) to assess inter-observer reproducibility for both rest and stress single-beat cine images; (3) reader 1 repeated the measurements on the same sample after 1.5 years to assess intra-observer reproducibility; (4) both readers independently evaluated inter-visit reproducibility in 15 healthy subjects, comparing rest and stress imaging between two visits conducted 1 year apart.

2.9. Statistical analysis

Continuous variables were presented as mean ± standard deviations [95% confidence interval (CI)]. Inter-observer and scan/rescan reproducibility were evaluated using the intraclass correlation coefficient (ICC). Correlation coefficients were interpreted as follows: excellent (0.9–1.0), good (0.75–0.89), fair (0.51–0.74), and poor (0.0–0.50) agreement [39]. All measurement agreements were assessed using Bland-Altman analysis, linear regression, and Pearson correlation. P-values were calculated using Student's t-test or Mann-Whitney test, as appropriate. All tests of significance were two-sided and assessed at $\alpha < 0.05$. Subjective diagnostic and image quality assessments were evaluated using descriptive statistics, with agreement and consistency across quality categories reported for the four readers. Statistical analyses were performed using Python (version 3.12, Wilmington, Delaware) in the PyCharm 2024.1 environment (JetBrains s.r.o., Prague, Czech Republic) and SPSS (version 29, IBM Corp., Armonk, New York).

3. Results

3.1. Participants

A total of 141 subjects were scanned, with five scans (3.5%) excluded from analysis: three due to PVCs captured during stress imaging and two due to incomplete cycle capture that missed the ES phase (Fig. S2). This resulted in 136 subjects in the final analysis (54 ± 15 years; 67 men). Ninety-six subjects were in the patient cohort: 72 with HF across all HF types and 24 undergoing evaluations for dyspnea of unclear etiology. The remaining 40 subjects were healthy controls. A total of 15 healthy subjects underwent a second Ex-CMR scan within 18 months (mean time between scans: 11.9 months [range 9.1–16.6 months]). Baseline characteristics are summarized in Table 2.

3.2. Image examples and scan time

Media 1A-B, 2A-B, 3A-B, and 4A-B represent full-stack cine acquisitions of rest and stress images in a healthy female, a patient with

reduced LVEF, a patient with wall motion abnormality (WMA), and a patient with 85% maximum age-predicted heart rate (MPHR), respectively. Fig. 4 shows examples of rest and stress single-beat cine images for a patient with HF. We acquired 14 ± 1 slices per subject and acquisition with a scan time of 30 ± 4 s per acquisition. The number of slices was higher than we typically acquire during rest to accommodate significant breathing motion post-exercise and likely motion of the subject during exercise.

Supplementary material related to this article can be found online at doi:10.1016/j.jocmr.2025.101901.

3.3. Exercise performance

Table 3 presents the healthy and patient cohorts' exercise performance and hemodynamic response. Both subgroups experienced increased blood pressure and HR during exercise, reaching 69 ± 7% of MPHR in the healthy cohort and 68 ± 11% in the patient cohort. The ΔHR (%) was 79 ± 30% for the healthy cohort and 64 ± 30% for the patient cohort. The rate pressure product increased from 7802 mmHg·bpm at rest to 17,726 mmHg·bpm at stress in the healthy cohort and from 7955 mmHg·bpm to 16,886 mmHg·bpm in the patient cohort (female: 17,653 mmHg·bpm; male: 16,120 mmHg·bpm). Fig. S3 shows the subjective exercise intensity assessments, with 63% of the healthy cohort and 64% of the patient cohort rating the exercise intensity as “hard” or “very hard.” Table 3 presents repeat exercise performance and hemodynamic responses for 15 healthy subjects during visits 1 and 2. The maximum workload achieved was 76 ± 18 W in visit 1 and 74 ± 20 W in visit 2 ($p = 0.801$). The MPHR reached 67 ± 8% in visit 1 and 67 ± 10% in visit 2 ($p = 0.894$).

3.4. Qualitative assessment

Fig. 5A shows the descriptive results of subjective diagnostic quality assessments. Rest single-beat cine was evaluated as diagnostic in 135/136 (99%), 135/136 (99%), 135/136 (99%), and 126/136 (93%) of subjects by readers 1, 2, 3, and 4, respectively. The same readers evaluated stress single-beat cine as diagnostic in 133/136 (98%), 131/136 (96%), 112/136 (82%), and 89/136 (65%) of subjects. Reader 4 rated 45/136 (33%) of cines as non-confident and only 2/136 (2%) as non-diagnostic. Reader agreement on diagnostic quality was assessed, revealing that 125 out of 136 (92%) rest single-beat and 80 out of 136 (59%) stress single-beat cines were consistently categorized as diagnostic by all readers. However, for the stress cines, agreement among readers with prior training in single-beat Ex-CMR cine analysis (readers 1 and 2) was higher, with 129 out of 136 (95%) categorized as diagnostic.

Fig. 5B shows the descriptive results of subjective image quality assessments. Rest single-beat cine was evaluated as having good quality in 133/136 (98%), 135/136 (99%), 135/136 (99%), and 136/136 (100%) of subjects by readers 1, 2, 3, and 4, respectively. Stress single-beat cine was evaluated as having good quality in 106/136 (78%), 109/136 (80%), 100/136 (74%), and 107/136 (79%) of subjects by readers 1, 2, 3, and 4, respectively. Endocardial border tracing was deemed feasible, meeting our good or adequate image quality criteria in 100%, 100%, 99%, and 99% of stress single-beat images by readers 1, 2, 3, and 4, respectively. Reader agreement on image quality was also assessed, revealing that 132 out of 136 (97%) of rest single-beat and 79 out of 136 (58%) of stress single-beat cines were consistently rated as having good image quality by all readers. However, for the stress cines, agreement among readers with prior training in single-beat Ex-CMR cine analysis (readers 1 and 2) was higher, with 104/136 (76%).

The primary artifact detected in the study was blurring. Additionally, expert readers noted other artifacts, including metal artifacts from coronary artery bypass graft or MitraClip, and chemical shift artifacts. The prevalence of incidents where the image artifact impacted image quality was minimal. For diagnostic confidence, the impact was less than 2% for reader 1, 4% for reader 2, 18% for reader 3%, and 35% for reader 4 (Fig. 5).

3.5. Quantitative assessment and reproducibility

Table S2 shows ICC of two readers for biventricular measurements in 41 out of 136 (30%). For rest single-beat cine measurements, readers had excellent agreement for calculations of LV and RV parameters, including EDV, ESV, EF, and SV with ICCs ranging from 0.91 (95% CI [0.84, 0.96]) for assessments of RVEF to 1.0 (95% CI [0.99, 1.0]) for LVEDV measurements at rest. ICCs for stress single-beat cine revealed good to excellent agreement ranging from 0.88 (95% CI [0.77, 0.94]) for RVSV to 0.99 (95% CI [0.99, 1.0]) for LVEDV measurements. Fig. 6 shows the variation of derived measurements by both readers in LVEF and RVEF assessments for rest and stress cines. Intra-observer assessment showed excellent reproducibility for all parameters (Table S2).

Table 4 summarizes the scan-rescan reproducibility of rest and stress biventricular measurements evaluated by both readers, demonstrating excellent inter-visit reproducibility. ICCs of reader 1 ranged from 0.96 (95% CI [0.90, 0.99]) to 1.0 (95% CI [0.99, 1.0]). For reader 2, ICCs of individual measurements ranged from 0.96 (95% CI [0.88, 0.99]) to 1.0 (95% CI [1.0, 1.0]).

Figs. 7 and 8 show the agreement of individual biventricular measurements at both visits as regression plots for readers 1 and 2. The coefficient of determination R^2 was at least 0.92 ($p < 0.001$) for LV parameters derived from rest and stress single-beat cines and 0.95 ($p < 0.001$) for RV parameters. As noted in Table S3, the absolute bias of measurements at the two visits was low, with no

Table 2
Baseline clinical and CMR characteristics.

Characteristics	All (n = 136)	Patients (n = 96)	Healthy (n = 40)
Demographics			
Age (years)	54 ± 15	58 ± 13	45 ± 16
Male n (%)	67 (49%)	48 (50%)	19 (48%)
Height (cm)	171 ± 9	171 ± 9	169 ± 9
Weight (kg)	80 ± 17	85 ± 16	69 ± 14
BMI (kg/m^2)	28 ± 6	29 ± 5	24 ± 3
Heart rate (bpm)	66 ± 11	65 ± 12	66 ± 9
CV conditions			
Heart failure*	72 (53%)	72 (75%)	0
Dyspnea unclear etiology	24 (18%)	24 (25%)	0
Hypertension	53 (39%)	53 (55%)	0
Atrial fibrillation	14 (10%)	14 (15%)	0
Coronary artery disease	29 (21%)	29 (30%)	0
Diabetes	13 (10%)	13 (14%)	0
Dyslipidemia	45 (33%)	45 (47%)	0
CMR			
LVEDV (mL)	165 ± 44	173 ± 48	145 ± 30
LVESV (mL)	74 ± 34	81 ± 37	61 ± 17
LVSV (mL)	90 ± 22	93 ± 23	84 ± 15
LVEF (%)	56 ± 9	55 ± 10	58 ± 4
LV-Mass (g)	97 ± 31	102 ± 34	86 ± 19
RVEDV (mL)	164 ± 42	169 ± 45	155 ± 33
RVESV (mL)	78 ± 27	80 ± 30	73 ± 20
RVSV (mL)	87 ± 8	89 ± 21	82 ± 15
RVEF (%)	53 ± 6	53 ± 7	53 ± 4

Continuous data are shown as mean ± SD; categorical data as number (%)
BMI body mass index, *CMR* cardiovascular magnetic resonance, *CV* cardiovascular, *EDV* end-diastolic volume, *EF* ejection fraction, *ESV* end-systolic volume, *LV* left ventricle, *RV* right ventricle, *SD* standard deviation, *SV* stroke volume
CMR data in this table are derived from rest single-beat cine, which has been previously compared with conventional technique
* 72 heart failure across all subgroups defined by guidelines [14]

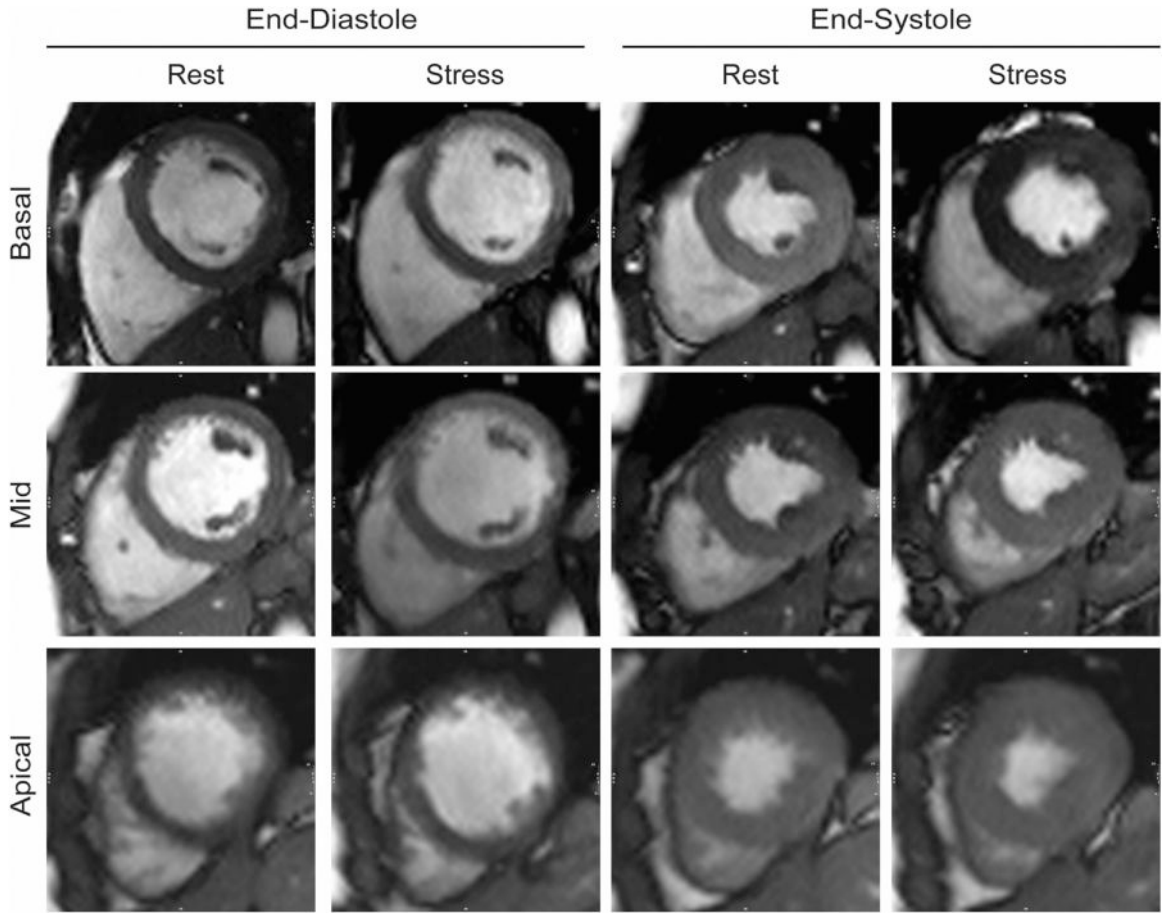

Fig. 4. Example of rest (HR = 59 bpm) and stress imaging (HR = 88 bpm) using single-beat cine acquisition in a patient with heart failure, illustrating three representative slices acquired from the basal, mid-ventricular, and apical regions. Minimal blurring in stress single-beat cine is attributed to cardiorespiratory motion artifacts. *HR* heart rate

Table 3
Exercise performance and hemodynamic response in all participants.

	Main cohorts		Scan/rescan reproducibility	
	Healthy (n = 40)	Patients (n = 96)	Visit 1 (n = 15)	Visit 2 (n = 15)
Response to exercise				
Duration (min)	9.3 ± 1.5	9.0 ± 1.7	9 ± 1.7	9 ± 1.2
Max. workload (W)	73 ± 17	57 ± 17	76 ± 18	74 ± 20
Absolute ΔHR (bpm)	52 ± 15	42 ± 17	46 ± 10	48 ± 15
Relative ΔHR (%)	79 ± 30	64 ± 30	67 ± 15	73 ± 23
(%) of max predicted HR	69 ± 7	68 ± 11	67 ± 8	67 ± 10
Δ systolic BP (mmHg)	33 ± 14	38 ± 16	34 ± 14	36 ± 8
Δ diastolic BP (mmHg)	15 ± 8	17 ± 13	15 ± 7	23 ± 12
Rate pressure product	17,726 ± 3169	16,886 ± 3586	16,613 ± 3439	16,737 ± 4020

Continuous data are shown as mean ± SD; categorical data as number (%)
BP blood pressure, *HR* heart rate, *SD* standard deviation
Rate pressure product = HR * systolic BP

significant differences in the scan-rescan bias between both readers (all p > 0.878).

Fig. 9 shows measurements for Rest1, Rest2, and Stress imaging during one visit, illustrating measurable volumetric and functional changes triggered by exercise, with an MPHR of 67 ± 10%.

4. Discussion

This study demonstrates that the proposed Ex-CMR single-beat cine and analysis workflow delivers highly reproducible measurements of biventricular volumetric and functional assessments, ensuring accurate endocardial tracing.

In single-beat cine images, a lower flip angle of 26 was used due to specific absorption rate constraints. A lower flip angle in the balanced steady-state free precession sequence reduces the blood-myocardium contrast. In our study, reader 4 had no prior experience analyzing single-beat Ex-CMR, resulting in a 33% non-confidence rate for stress images when interpreting diagnostic quality based on cine videos. In contrast, readers 1, 2, and 3, who had prior Ex-CMR experience, demonstrated substantially lower non-confidence rates. Familiarity with free-breathing acquisitions and cardiac phase inconsistencies was essential for increasing readers' confidence, as these factors differ from conventional CMR [37]. This highlights the importance of familiarization with new imaging techniques. However,

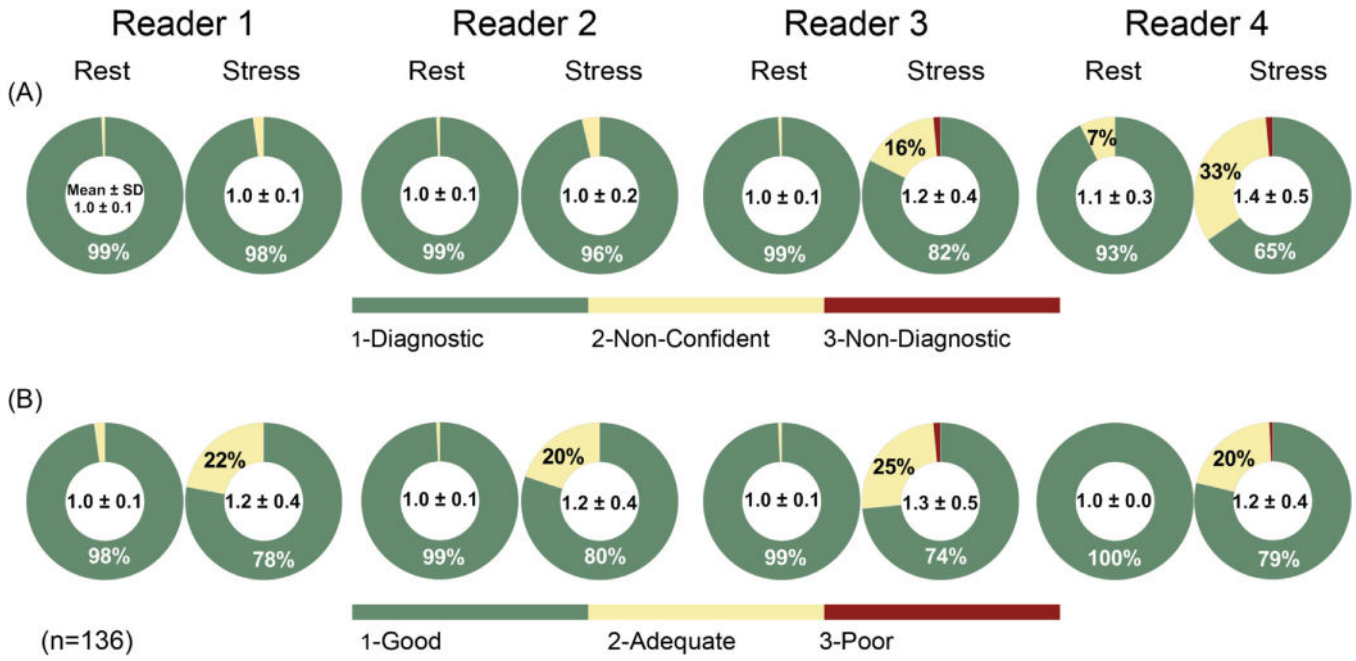

Fig. 5. Qualitative assessment. (A) Diagnostic and (B) image quality assessments of both rest and stress cine acquisitions across all subjects (n = 136). Four independent readers rated the data using a 3-point Likert scale for (A) diagnostic quality (1: diagnostic; 2: non-confident; 3: non-diagnostic) and a 3-point Likert scale for (B) image quality (1: good; 2: adequate; 3: poor). Note: For values less than 5%, only color-coding is provided

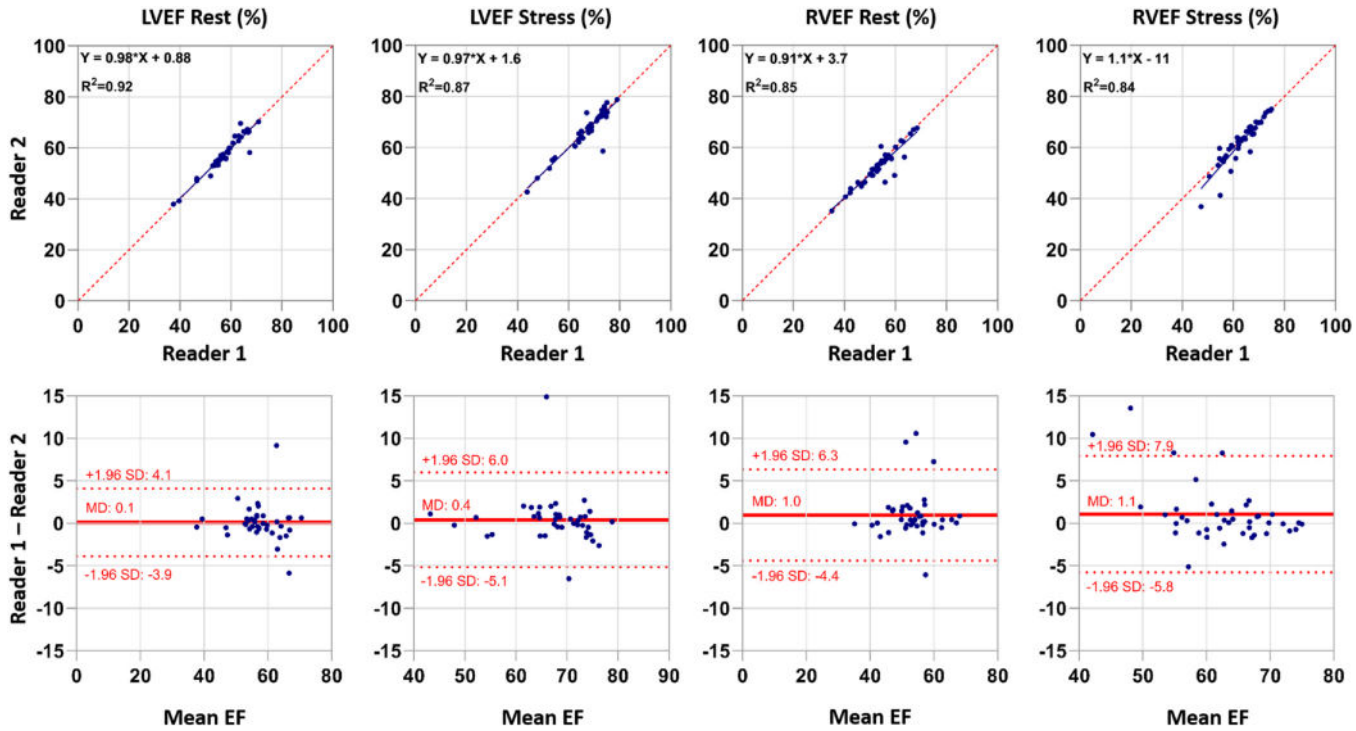

Fig. 6. Inter-observer agreement for LV and RVEF obtained from rest and stress imaging in 41 (30%) of the acquired data. The top row shows regression plots illustrating the agreement between both readers. The bottom row displays Bland-Altman plots of the bias between the two readers. *EF* ejection fraction, *LV* left ventricular, *MD* mean difference, *RV* right ventricular, *SD*, standard deviation

reader 4's image quality assessment, based on static images, was comparable to or even slightly better than that of the other three readers.

Although the image quality of stress Ex-CMR cines was lower than resting images, the endocardial borders were deemed feasible to delineate based on the quality score definition, as assessed by four experts. From a clinical perspective on volume assessment, the quality of endocardial borders is crucial for accurate volumetric and functional measurements [40] and was well-preserved in Ex-CMR single-beat cines. This notice gains additional importance as earlier studies reported difficulties in volumetric assessments if endocardium becomes less identifiable at increasing HRs [6] and lower temporal resolutions [18]. Beyond that, no systematic reporting on the quality of Ex-CMR acquisitions has been published to date [41]. Beyond image quality, systematic studies on reproducibility of biventricular measurements during exercise are required to improve confidence in reported volumetric and functional parameters during exercise.

Table 4
ICCs for inter-visit reproducibility.

*Scan-rescan reproducibility between visit 1 (V1) and visit 2 (V2) 1 year apart (n = 15)

Reader 1				
	LVEDV	**LVESV**	**LVEF**	**LVSV**
Rest V1 vs V2	1.0 [0.99, 1.0]	1.0 [0.99, 1.0]	0.98 [0.94, 1.0]	1.0 [0.99, 1.0]
Stress V1 vs V2	1.0 [0.99, 1.0]	0.99 [0.98, 1.0]	0.98 [0.95, 0.99]	0.99 [0.98, 1.0]
	RVEDV	**RVESV**	**RVEF**	**RVSV**
Rest V1 vs V2	0.99 [0.96,1.0]	0.99 [0.97,1.0]	0.97 [0.92, 0.99]	0.97 [0.91, 0.99]
Stress V1 vs V2	0.97 [0.93, 0.99]	0.97 [0.93, 0.99]	0.96 [0.90, 0.99]	0.97 [0.91, 0.99]
Reader 2				
	LVEDV	**LVESV**	**LVEF**	**LVSV**
Rest V1 vs V2	1.0 [1.0, 1.0]	0.99 [0.98, 1.0]	0.96 [0.88, 0.99]	1.0 [0.99, 1.0]
Stress V1 vs V2	1.0 [1.0, 1.0]	1.0 [0.99, 1.0]	0.99 [0.97, 1.0]	1.0 [0.99, 1.0]
	RVEDV	**RVESV**	**RVEF**	**RVSV**
Rest V1 vs V2	1.0 [1.0, 1.0]	1.0 [1.0, 1.0]	0.99 [0.97, 1.0]	0.99 [0.98, 1.0]
Stress V1 vs V2	1.0 [1.0, 1.0]	1.0 [0.99, 1.0]	0.98 [0.95, 0.99]	0.99 [0.97, 1.0]

EDV end-diastolic volume, *EF* ejection fraction, *ESV* end-systolic volume, *ICC* intraclass correlation coefficient, *LV* left ventricle, *RV* right ventricle, *SV* stroke volume [95% confidence interval]
Data represent ICC values with 95% CI.
* Scan/rescan reproducibility was assessed on 38% (n = 15) of subjects from the healthy cohort (n = 40)

In our study, biventricular measurements in REGAIN-enhanced Ex-CMR single-beat cine showed excellent reproducibility, and repeated Ex-CMR acquisitions showed high agreement with the baseline scan. The lower inter-observer agreement on RV function compared to LV function is an established observation from conventionally gated cine images at rest [42] as the complex shape of the RV, especially in basal regions, challenges accurate endocardial delineation more than in the LV [43]. Furthermore, the observed bias for functional measurements is

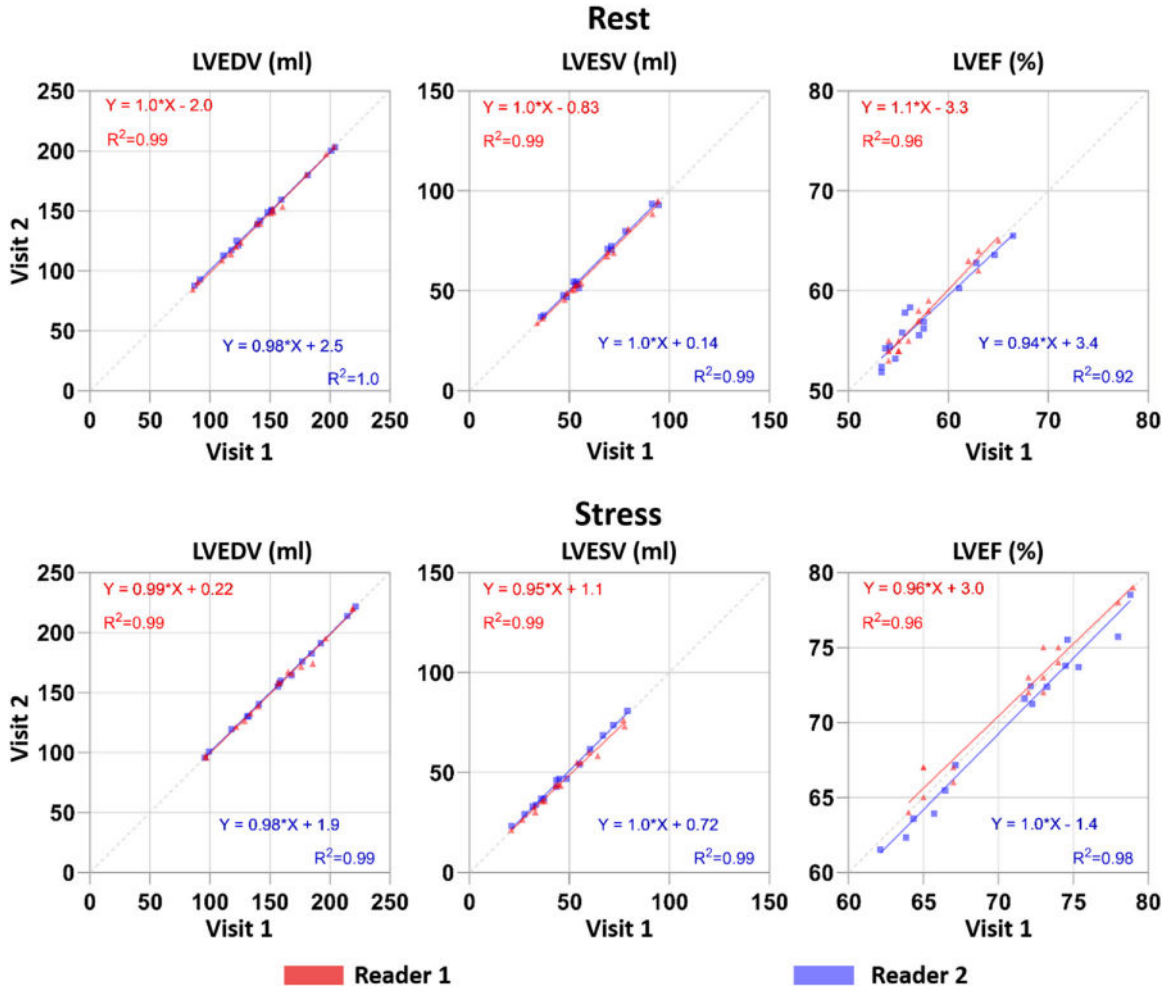

Fig. 7. Regression plots of LV volumetric measurements agreement between visits 1 and 2 in two readers. Displayed are regression plots of the inter-visit agreement LVEDV, LVESV, and LVEF measurements at rest (top row) and during exercise stress (bottom row). Red indicates measurements by reader 1, blue indicates measurements by reader 2. *EDV* end-diastolic volume, *EF* ejection fraction, *ESV* end-systolic volume, *LV* left ventricular

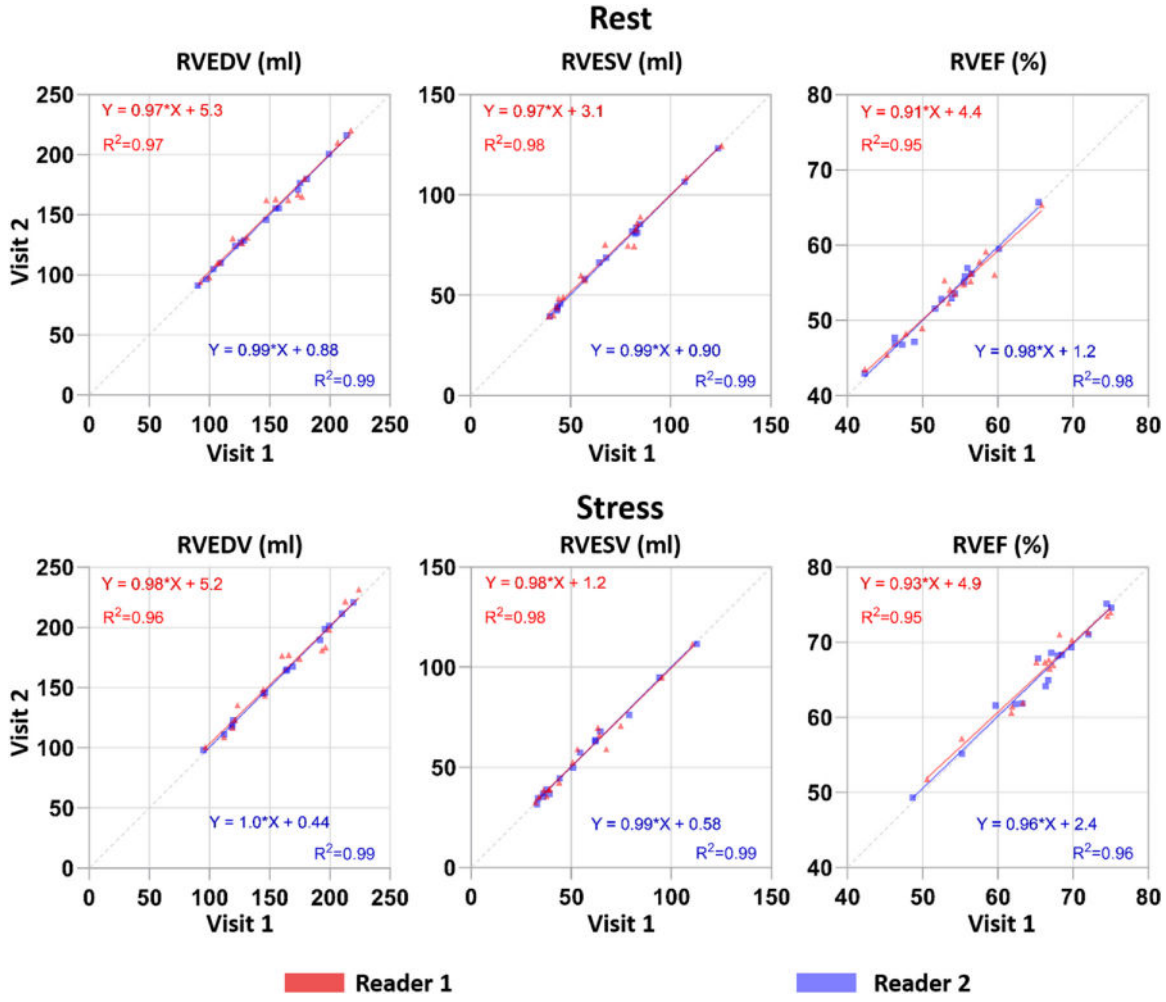

Fig. 8. Regression plots of agreement of RV volumetric measurements between visits 1 and 2 in two readers. Displayed are regression plots of the inter-visit agreement RVEDV, RVESV, and RVEF measurements at rest (top row) and during exercise stress (bottom row). Red indicates measurements by reader 1, blue indicates measurements by reader 2. *EDV* end-diastolic volume, *EF* ejection fraction, *ESV* end-systolic volume, *RV* right ventricular

small when interpreted in a clinical context. These findings align with earlier data showing good inter-observer agreement of volumetric and functional assessments during exercise stress [6,7,17,18,44,45]. However, prior analyses mainly were conducted in small patient populations or subsets of the study cohort and often focused solely on the reproducibility of LVSV rather than on individual biventricular measures of volume and function during exercise. This limits existing confidence in Ex-CMR measurements and may explain why previous sequences have not been adopted by vendors.

Earlier studies on inter-scan repeatability also paralleled the observed agreement between both scans but reported higher absolute variability of measurements [17,44]. This might be attributed to actual physiological changes or differences in exercise performance rather than to the observer. Therefore, this study only included healthy subjects for assessing inter-visit reproducibility to ensure stability in cardiac function, as the patient population may experience variations over a year. The excellent inter-visit reproducibility of two independent readers highlights that cardiac contouring and post-processing do not impose additional inaccuracies over other unknown variables when performing Ex-CMR. However, it must be emphasized that those results were achieved by readers who have been adequately trained and followed a systematic post-processing and quality control workflow. The positive effect of training on the accuracy of cardiac functional measurement is well-established [46]. This was underscored by the observation that readers with prior experience in Ex-CMR imaging assigned higher quality scores to Ex-CMR single-beat cines than CMR readers with less familiarization with Ex-CMR acquisitions. Therefore, systematic training and re-retaining of (experienced) CMR readers are essential to derive accurate and reproducible measurements from Ex-CMR images and advance this field toward clinical application in targeted patient populations.

The exercise intensity in our study was set at a moderate-to-intense effort level, with the average MPHR at 69%, which is below the typically expected threshold of 85% for exercise protocols aimed at detecting CAD. However, volumetric and functional changes are well documented at moderate exercise intensities using the supine bike, which results in a greater increase in venous return and preload compared to upright exercise [7]. Our results demonstrated measurable volumetric and functional changes from rest to stress. Exploring cardiac adaptation to increased preload while still experiencing an increase in afterload is particularly relevant for future investigations into functional reserve in patient populations, including those with HF and limited functional capacity, or patients with LV outflow tract obstruction, where high-intensity exercise is generally not recommended in research settings.

In our study, while regional WMA were generally trackable as assessed by a single reader (reader 1), we did not aim to conduct a systematic evaluation of WMA detection, as this was beyond the scope of the study. We acknowledge, however, that the spatial resolution and temporal fidelity of single-beat images are influenced by several factors—including incomplete steady-state contrast, through-plane motion, CS reconstruction based on a limited number of cardiac phases,

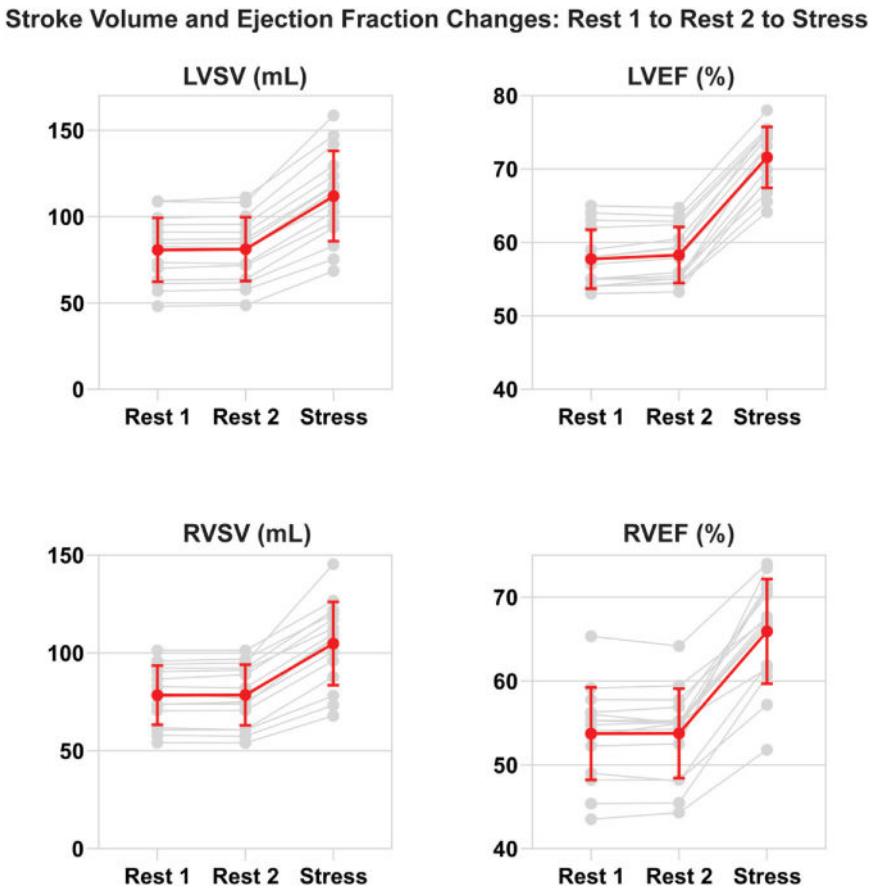

Fig. 9. Measurements of biventricular (LV/RV) stroke volume (SV) and ejection fraction (EF) for Rest1, Rest2, and Stress imaging during one visit, illustrating measurable volumetric and functional changes triggered by exercise, with an MPHR of 67 ± 10%. *MPHR* maximum age-predicted heart rate, *LV* left ventricular, *RV* right ventricular

and truncated phase-encoding resolution—which may affect the sensitivity for detecting regional WMA. These complex interactions can result in artifacts, such as myocardial thinning or suboptimal motion visualization.

5. Limitations

The present work is a single-center study in an experienced CMR lab. The reproducibility of measurements might be lower for less-trained readers. The performance of the proposed single-beat cine has not been tested at other field strengths or on CMR scanners or exercise equipment from different vendors. The post-processing workflow has only been adjusted for a single commercially available post-processing software. Even though the workflow can be adopted in other software, performance and results might differ. Patients with arrhythmia have not been systematically evaluated. Acquisitions at rest and during stress were obtained during free breathing without respiratory motion compensation, leading to motion between slices and potential errors in volume quantification. We did not use a respiratory trigger for data acquisition, resulting in through-plane motions that were not accounted for in our implementation. However, the proposed workflow systematically accounts for through-plane motion, potential RR variations or PVCs, and large respiratory compensation to minimize inaccuracies. Nonetheless, minor errors in volumetric measurements due to respiratory motion and phase inconsistency remain. Further studies are warranted to investigate solutions such as respiratory-triggered imaging or external motion sensors.

Although reader 2 was blinded to the results of reader 1, they were trained by reader 1 in the utilization of the post-processing and quality control workflow and reading of the DL-enhanced images. While this may introduce a bias toward improved repeatability, it also highlights the benefits of structured training and workflows.

Although our study demonstrated the feasibility of implementing single-beat cine for quantifying biventricular indices with intact endocardial tracing in stress images and excellent reproducibility. We did not systematically evaluate single-beat cine for exercise-induced regional WMA, as we had excluded patients with CAD who required revascularization or imminent intervention. Further studies in targeted patient populations with suspected CAD or those undergoing work-up for CAD, or a wide spectrum of WMA are needed to evaluate this sequence for detecting exercise-induced regional abnormalities and assess its readiness for full clinical implementation. Furthermore, we acknowledge that a study investigating CAD would require a more intense exercise protocol, simulating an MPHR of ≥ 85%, which was not achieved in our study.

Further optimization of the sequence may allow for higher flip angles to improve contrast, which may be explored in future studies.

6. Conclusion

We evaluated a free-breathing, high-spatiotemporal resolution Ex-CMR single-beat cine for evaluation of LV and RV systolic function and volumes. It demonstrated excellent reproducibility in quantifying biventricular volumetric and functional parameters across readers and repeated scans. The method preserved diagnostic and image quality, enabling precise endocardial border delineation during stress imaging.

Funding

Reza Nezafat receives grant funding from the National Institutes of Health (NIH) R01 HL158077 (Bethesda, Maryland).

Author contributions

FG conceptualized the study design, developed the analysis workflow and quality scoring criteria, performed image and data analysis, and prepared and revised the manuscript. **AS** contributed to reproducibility analyses, scoring qualitative assessments and writing. **MAM** was involved in sequence development and study design. **JR** and **JAS** were involved in recruiting, consenting, and data curation. **KA**, **SJ** and **PP** were involved in data collection. **CWH** and **CWT** scored qualitative assessments. **WJM** contributed to study design, data interpretation, and manuscript revision. **RN** supervised the study and contributed to the study design, data interpretation, funding, and manuscript revision. All authors critically revised the paper and have read and approved the final manuscript.

Ethics approval and consent

This study was approved by the Beth Israel Deaconess Medical Center Institutional Review Board and was compliant with the Health Insurance Portability and Accountability Act.

Consent for publication

Written informed consent was obtained from each prospective participant.

Availability of data and materials

Source codes for REGAIN are available online (https://github.com/HMS-CardiacMR/REGAIN).

Declaration of competing interests

The authors report no conflict of interest.

Appendix A. Supporting information

Supplementary data associated with this article can be found in the online version at doi:10.1016/j.jocmr.2025.101901.

References

[1] Niezen RA, Doornbos J, van der Wall EE, de Roos A. Measurement of aortic and pulmonary flow with MRI at rest and during physical exercise. J Comput Assist Tomogr 1998;22:194–201. https://doi.org/10.1097/00004728-199803000-00006.

[2] Craven TP, Tsao CW, La Gerche A, Simonetti OP, Greenwood JP. Exercise cardiovascular magnetic resonance: development, current utility and future applications. J Cardiovasc Magn Reson 2020;22:65. https://doi.org/10.1186/s12968-020-00652-w.

[3] Trankle CR, Canada JM, Jordan JH, Truong U, Hundley WG. Exercise cardiovascular magnetic resonance: a review. J Magn Reson Imaging 2022;55:720–54. https://doi.org/10.1002/jmri.27580.

[4] Claessen G, Schnell F, Bogaert J, Claeys M, Pattyn N, De Buck F, et al. Exercise cardiac magnetic resonance to differentiate athlete's heart from structural heart disease. Eur Heart J Cardiovasc Imaging 2018;19:1062–70. https://doi.org/10.1093/ehjci/jey050.

[5] Gusso S, Pinto T, Baldi JC, Derraik JGB, Cutfield WS, Hornung T, et al. Exercise training improves but does not normalize left ventricular systolic and diastolic function in adolescents with type 1 diabetes. Diabetes Care 2017;40:1264–72. https://doi.org/10.2337/dc16-2347.

[6] Gerche A, Claessen G, Van de Bruaene A, Pattyn N, Van Cleemput J, Gewillig M, et al. Cardiac MRI: a new gold standard for ventricular volume quantification during high-intensity exercise. Circ Cardiovasc Imaging 2013;6:329–38. https://doi.org/10.1161/circimaging.112.980037.

[7] Le TT, Bryant JA, Ang BWY, Pua CJ, Su B, Ho PY, et al. The application of exercise stress cardiovascular magnetic resonance in patients with suspected dilated cardiomyopathy. J Cardiovasc Magn Reson 2020;22:10. https://doi.org/10.1186/s12968-020-0598-4.

[8] Pinto TE, Gusso S, Hofman PL, Derraik JG, Hornung TS, Cutfield WS, et al. Systolic and diastolic abnormalities reduce the cardiac response to exercise in adolescents with type 2 diabetes. Diabetes Care 2014;37:1439–46. https://doi.org/10.2337/dc13-2031.

[9] Backhaus SJ, Lange T, George EF, Hellenkamp K, Gertz RJ, Billing M, et al. Exercise stress real-time cardiac magnetic resonance imaging for noninvasive characterization of heart failure with preserved ejection fraction: the HFpEF-Stress trial. Circulation 2021;143:1484–98. https://doi.org/10.1161/circulationaha.120.051542.

[10] Claessen G, La Gerche A, Wielandts JY, Bogaert J, Van Cleemput J, Wuyts W, et al. Exercise pathophysiology and sildenafil effects in chronic thromboembolic pulmonary hypertension. Heart 2015;101:637–44. https://doi.org/10.1136/heartjnl-2014-306851.

[11] Raman SV, Dickerson JA, Mazur W, Wong TC, Schelbert EB, Min JK, et al. Diagnostic performance of treadmill exercise cardiac magnetic resonance: the prospective, multicenter exercise CMR's accuracy for cardiovascular stress testing (EXACT) Trial. J Am Heart Assoc 2016;5:e003811. https://doi.org/10.1161/JAHA.116.003811.

[12] Bellenger NG, Burgess MI, Ray SG, Lahiri A, Coats AJ, Cleland JG, et al. Comparison of left ventricular ejection fraction and volumes in heart failure by echocardiography, radionuclide ventriculography and cardiovascular magnetic resonance; are they interchangeable? Eur Heart J 2000;21:1387–96. https://doi.org/10.1053/euhj.2000.2011.

[13] Gulsin GS, Singh A, McCann GP. Cardiovascular magnetic resonance in the evaluation of heart valve disease. BMC Med Imaging 2017;17:67. https://doi.org/10.1186/s12880-017-0238-0.

[14] Heidenreich PA, Bozkurt B, Aguilar D, Allen LA, Byun JJ, Colvin MM, et al. 2022 AHA/ACC/HFSA Guideline for the management of heart failure: a report of the American College of Cardiology/American Heart Association Joint Committee on Clinical Practice Guidelines. Circulation 2022;145:e895–1032. https://doi.org/10.1161/cir.0000000000001063.

[15] Roest AA, Helbing WA, Kunz P, van den Aardweg JG, Lamb HJ, Vliegen HW, et al. Exercise MR imaging in the assessment of pulmonary regurgitation and biventricular function in patients after tetralogy of Fallot repair. Radiology 2002;223:204–11. https://doi.org/10.1148/radiol.2231010924.

[16] Roest AA, Kunz P, Lamb HJ, Helbing WA, van der Wall EE, de, Roos A. Biventricular response to supine physical exercise in young adults assessed with ultrafast magnetic resonance imaging. Am J Cardiol 2001;87:601–5. https://doi.org/10.1016/s0002-9149(00)01438-7.

[17] Le TT, Bryant JA, Ting AE, Ho PY, Su B, Teo RC, et al. Assessing exercise cardiac reserve using real-time cardiovascular magnetic resonance. J Cardiovasc Magn Reson 2017;19:7. https://doi.org/10.1186/s12968-017-0322-1.

[18] Lurz P, Muthurangu V, Schievano S, Nordmeyer J, Bonhoeffer P, Taylor AM, et al. Feasibility and reproducibility of biventricular volumetric assessment of cardiac function during exercise using real-time radial k-t SENSE magnetic resonance imaging. J Magn Reson Imaging 2009;29:1062–70. https://doi.org/10.1002/jmri.21762.

[19] Hundley WG, Bluemke DA, Finn JP, Flamm SD, Fogel MA, Friedrich MG, et al. ACCF/ACR/AHA/NASCI/SCMR 2010 expert consensus document on cardiovascular magnetic resonance: a report of the American College of Cardiology Foundation Task Force on Expert Consensus Documents. J Am Coll Cardiol 2010;55:2614–62. https://doi.org/10.1016/j.jacc.2009.11.011.

[20] Curione D, Ciliberti P, Monti CB, Capra D, Bordonaro V, Ciancarella P, et al. Compressed sensing cardiac cine imaging compared with standard balanced steady-state free precession cine imaging in a pediatric population. Radiol Cardiothorac Imaging 2022;4:e210109. https://doi.org/10.1148/ryct.210109.

[21] Lin ACW, Strugnell W, Riley R, Schmitt B, Zenge M, Schmidt M, et al. Higher resolution cine imaging with compressed sensing for accelerated clinical left ventricular evaluation. J Magn Reson Imaging 2017;45:1693–9. https://doi.org/10.1002/jmri.25525.

[22] Craft J, Li Y, Nashta NF, Weber J. Comparison between compressed sensing and segmented cine cardiac magnetic resonance: a meta-analysis. BMC Cardiovasc Disord 2023;23:473. https://doi.org/10.1186/s12872-023-03426-1.

[23] Ahmed AH, Qureshi IM, Shah JA, Zaheer M. Motion correction based reconstruction method for compressively sampled cardiac MR imaging. Magn Reson Imaging 2017;36:159–66. https://doi.org/10.1016/j.mri.2016.10.008.

[24] Cruz G, Hammernik K, Kuestner T, Velasco C, Hua A, Ismail TF, et al. Single-heartbeat cardiac cine imaging via jointly regularized nonrigid motion-corrected reconstruction. NMR Biomed 2023;36:e4942. https://doi.org/10.1002/nbm.4942.

[25] Feng L, Axel L, Chandarana H, Block KT, Sodickson DK, Otazo R. XD-GRASP: Golden-angle radial MRI with reconstruction of extra motion-state dimensions using compressed sensing. Magn Reson Med 2016;75:775–88. https://doi.org/10.1002/mrm.25665.

[26] Usman M, Atkinson D, Odille F, Kolbitsch C, Vaillant G, Schaeffter T, et al. Motion corrected compressed sensing for free-breathing dynamic cardiac MRI. Magn Reson Med 2013;70:504–16. https://doi.org/10.1002/mrm.24463.

[27] Hauptmann A, Arridge S, Lucka F, Muthurangu V, Steeden JA. Real-time cardiovascular MR with spatio-temporal artifact suppression using deep learning-proof of concept in congenital heart disease. Magn Reson Med 2019;81:1143–56. https://doi.org/10.1002/mrm.27480.

[28] Morales MA, Yoon S, Fahmy A, Ghanbari F, Nakamori S, Rodriguez J, et al. Highly accelerated free-breathing real-time myocardial tagging for exercise cardiovascular magnetic resonance. J Cardiovasc Magn Reson 2023;25:56. https://doi.org/10.1186/s12968-023-00961-w.

[29] Shen D, Ghosh S, Haji-Valizadeh H, Pathrose A, Schiffers F, Lee DC, et al. Rapid reconstruction of highly undersampled, non-Cartesian real-time cine k-space data using a perceptual complex neural network (PCNN). NMR Biomed 2021;34:e4405. https://doi.org/10.1002/nbm.4405.

[30] Morales MA, Assana S, Cai X, Chow K, Haji-Valizadeh H, Sai E, et al. An inline deep learning based free-breathing ECG-free cine for exercise cardiovascular magnetic resonance. J Cardiovasc Magn Reson 2022;24:47. https://doi.org/10.1186/s12968-022-00879-9.

[31] Demirel OB, Zhang C, Yaman B, Gulle M, Shenoy C, Leiner T, et al. High-fidelity database-free deep learning reconstruction for real-time cine cardiac MRI. Annu Int Conf IEEE Eng Med Biol Soc 2023;2023:1–4. https://doi.org/10.1109/embc40787.2023.10340709.

[32] Zucker EJ, Sandino CM, Kino A, Lai P, Vasanawala SS. Free-breathing accelerated cardiac MRI using deep learning: Validation in children and young adults. Radiology 2021;300:539–48. https://doi.org/10.1148/radiol.2021202624.
[33] Berggren K, Ryd D, Heiberg E, Aletras AH, Hedström E. Super-resolution cine image enhancement for fetal cardiac magnetic resonance imaging. J Magn Reson Imaging 2022;56:223–31. https://doi.org/10.1002/jmri.27956.
[34] Masutani EM, Bahrami N, Hsiao A. Deep learning single-frame and multiframe super-resolution for cardiac MRI. Radiology 2020;295:552–61. https://doi.org/10.1148/radiol.2020192173.
[35] Morales MA, Manning WJ, Nezafat R. Present and future innovations in AI and cardiac MRI. Radiology 2024;310:e231269. https://doi.org/10.1148/radiol.231269.
[36] Yoon S, Nakamori S, Amyar A, Assana S, Cirillo J, Morales MA, et al. Accelerated cardiac MRI cine with use of resolution enhancement generative adversarial inline neural network. Radiology 2023;307:e222878. https://doi.org/10.1148/radiol.222878.
[37] Ghanbari F, Morales MA, Street JA, Rodriguez J, Johnson S, Pierce P, et al. Free-breathing, highly accelerated, single-beat, multisection cardiac cine MRI with generative artificial intelligence. Radiol Cardiothorac Imaging 2025;7:e240272. https://doi.org/10.1148/ryct.240272.
[38] Chow K, Kellman P, Xue H. Prototyping image reconstruction and analysis with FIRE. SCMR 24th annual scientific sessions Virtual Meeting; 2021.
[39] Portney LG. Foundations of clinical research: applications to evidence-based practice. Philadelphia, PA: FA Davis Company; 2020.
[40] Clay S, Alfakih K, Messroghli DR, Jones T, Ridgway JP, Sivananthan MU. The reproducibility of left ventricular volume and mass measurements: a comparison between dual-inversion-recovery black-blood sequence and SSFP. Eur Radiol 2006;16:32–7. https://doi.org/10.1007/s00330-005-2853-3.
[41] Hundley WG, Bluemke D, Bogaert JG, Friedrich MG, Higgins CB, Lawson MA, et al. Society for Cardiovascular Magnetic Resonance guidelines for reporting cardiovascular magnetic resonance examinations. J Cardiovasc Magn Reson 2009;11:5. https://doi.org/10.1186/1532-429x-11-5.
[42] Grothues F, Moon JC, Bellenger NG, Smith GS, Klein HU, Pennell DJ. Interstudy reproducibility of right ventricular volumes, function, and mass with cardiovascular magnetic resonance. Am Heart J 2004;147:218–23. https://doi.org/10.1016/j.ahj.2003.10.005.
[43] Alfakih K, Plein S, Bloomer T, Jones T, Ridgway J, Sivananthan M. Comparison of right ventricular volume measurements between axial and short axis orientation using steady-state free precession magnetic resonance imaging. J Magn Reson Imaging 2003;18:25–32. https://doi.org/10.1002/jmri.10329.
[44] Chew PG, Swoboda PP, Ferguson C, Garg P, Cook AL, Ibeggazene S, et al. Feasibility and reproducibility of a cardiovascular magnetic resonance free-breathing, multi-shot, navigated image acquisition technique for ventricular volume quantification during continuous exercise. Quant Imaging Med Surg 2020;10:1837–51. https://doi.org/10.21037/qims-20-117.
[45] Steinmetz M, Stümpfig T, Seehase M, Schuster A, Kowallick J, Müller M, et al. Impaired exercise tolerance in repaired tetralogy of Fallot is associated with impaired biventricular contractile reserve: an exercise-stress real-time cardiovascular magnetic resonance study. Circ Cardiovasc Imaging 2021;14:e011823. https://doi.org/10.1161/circimaging.120.011823.
[46] Karamitsos TD, Hudsmith LE, Selvanayagam JB, Neubauer S, Francis JM. Operator induced variability in left ventricular measurements with cardiovascular magnetic resonance is improved after training. J Cardiovasc Magn Reson 2007;9:777–83. https://doi.org/10.1080/10976640701545073.